AGU PUBLICATIONS

JGR

Journal of Geophysical Research: Atmospheres

RESEARCH ARTICLE
10.1002/2015JD024566

This article is a companion to *Wang et al.* [2016] doi:10.1002/2015JD024556.

Key Points:
- Large (up to 12 ppbv N_2O_5) but infrequent nocturnal NOx outflow from the Pearl River Delta
- Average N_2O_5 uptake coefficients 0.014 ± 0.007, in line with residual layer measurements in the U.S.
- Daytime N_2O_5 follows predicted steady state but rapidly produces soluble nitrate in fog

Correspondence to:
S. S. Brown,
steven.s.brown@noaa.gov

Citation:
Brown, S. S., et al. (2016), Nighttime chemistry at a high altitude site above Hong Kong, *J. Geophys. Res. Atmos.*, *121*, 2457–2475, doi:10.1002/2015JD024566.

Received 24 NOV 2015
Accepted 5 FEB 2016
Accepted article online 11 FEB 2016
Published online 11 MAR 2016

Nighttime chemistry at a high altitude site above Hong Kong

Steven S. Brown[1,2], William P. Dubé[1,3], Yee Jun Tham[4], Qiaozhi Zha[4], Likun Xue[4], Steven Poon[4], Zhe Wang[4], Donald R. Blake[5], Wilson Tsui[6], David D. Parrish[1,3], and Tao Wang[4]

[1]Chemical Sciences Division, NOAA Earth System Research Laboratory, Boulder, Colorado, USA, [2]Department of Chemistry and Biochemistry, University of Colorado Boulder, Boulder, Colorado, USA, [3]Cooperative Institute for Research in Environmental Sciences, University of Colorado Boulder, Boulder, Colorado, USA, [4]Department of Civil and Environmental Engineering, Hong Kong Polytechnic University, Hong Kong, China, [5]Department of Chemistry, University of California, Irvine, California, USA, [6]PTC International Limited, Hong Kong, China

Abstract Nighttime reactions of nitrogen oxides influence ozone, volatile organic compounds, and aerosol and are thus important to the understanding of regional air quality. Despite large emissions and rapid recent growth of nitrogen oxide concentrations, there are few studies of nighttime chemistry in China. Here we present measurements of nighttime nitrogen oxides, NO_3 and N_2O_5, from a coastal mountaintop site in Hong Kong adjacent to the megacities of the Pearl River Delta region. This is the first study of nighttime chemistry from a site within the residual layer in China. Key findings include the following. First, highly concentrated urban NO_x outflow from the Pearl River Delta region was sampled infrequently at night, with N_2O_5 mixing ratios up to 8 ppbv (1 min average) or 12 ppbv (1 s average) in nighttime aged air masses. Second, the average N_2O_5 uptake coefficient was determined from a best fit to the available steady state lifetime data as $\gamma(N_2O_5) = 0.014 \pm 0.007$. Although this determination is uncertain due to the difficulty of separating N_2O_5 losses from those of NO_3, this value is in the range of previous residual layer determinations of N_2O_5 uptake coefficients in polluted air in North America. Third, there was a significant contribution of biogenic hydrocarbons to NO_3 loss inferred from canister samples taken during daytime. Finally, daytime N_2O_5 mixing ratios were in accord with their predicted photochemical steady state. Heterogeneous uptake of N_2O_5 in fog is determined to be an important production mechanism for soluble nitrate, even during daytime.

1. Introduction

The emissions and atmospheric chemistry of nitrogen oxides ($NO_x = NO + NO_2$) influence air quality and climate through their regulation of secondary pollutants such as ozone and aerosols. Nitrogen oxides undergo both photochemical (sunlight driven) and dark (requiring the absence of sunlight) chemical cycles. During daytime, they act as catalysts in the well-known mechanism for the production of tropospheric ozone. At night, they participate in a separate set of reactions that removes both ozone and nitrogen oxides from the atmosphere, initiates the oxidation of volatile organic compounds, serves as a source of secondary aerosol, and activates halogen species [*Brown and Stutz*, 2012]. The oxidation of NO_2 by O_3, which produces the nitrate radical, NO_3, initiates these chemical cycles.

$$NO_2 + O_3 \rightarrow NO_3 + O_2 \quad (1)$$

$$NO_3 + NO_2 \leftrightarrows N_2O_5 \quad (2)$$

$$NO_3 + VOC \rightarrow Products \quad (3)$$

$$N_2O_5 + H_2O(het) \rightarrow 2HNO_3 \quad (4)$$

$$N_2O_5 + Cl^-(het) \rightarrow ClNO_2 + NO_3^- \quad (5)$$

The nitrate radical is short lived during daytime due to its rapid photolysis and reaction with NO, both of which serve to regenerate NO_x and effectively reverse reaction (1). The NO_3 concentration increases during nighttime, together with that of dinitrogen pentoxide, N_2O_5, with which it is in thermal equilibrium via reaction (2). The nitrate radical is a strong oxidant of unsaturated hydrocarbons and reduced sulfur compounds. It is therefore highly reactive with biogenic hydrocarbons such as isoprene and monoterpenes in terrestrial environments [*Winer et al.*, 1984] and dimethyl sulfide in marine environments [*Platt et al.*, 1990]. Nighttime reactions of NO_3 with isoprene and monoterpenes may be an important mechanism for

production of secondary organic aerosol [*Pye et al*., 2010]. Dinitrogen pentoxide reacts via heterogeneous uptake to aerosol to yield soluble nitrate (HNO_3 or NO_3^-) or nitryl chloride, $ClNO_2$. The latter undergoes morning photolysis subsequent to its nighttime production and acts as a source of atomic chlorine radicals and NO_2. This mechanism recycles NO_2 that would otherwise be converted to soluble nitrate if all N_2O_5 uptake proceeded through reaction (4). The availability of aerosol phase chloride determines the competition between reactions (4) and (5) [*Bertram and Thornton*, 2009; *Roberts et al*., 2009]. Recent field studies have shown that $ClNO_2$ production is widespread and represents a large source of reactive halogens to the troposphere [*Thornton et al*., 2010].

Production of NO_3 via reaction (1) depends linearly on the mixing ratios of both O_3 and NO_2. Emissions of nitrogen oxides have been declining steadily in North America and Europe but increasing rapidly in Asia [*Hilboll et al*., 2013; *Russell et al*., 2012]. The recent trend in satellite-derived NO_2 column over large cities in China shows an increase of +5–10% yr^{-1} [*Hilboll et al*., 2013]. Surface ozone concentrations have been declining across broad areas of the United States in response to declining NO_x emissions [*Cooper et al*., 2012; *Simon et al*., 2014]. Reported O_3 data in China are not as extensive as those in the U.S. and Europe, but reports of surface ozone in China suggest large ozone production downwind of Beijing [*Wang et al*., 2006] but only modest trends within the city itself [*Tang et al*., 2009]. In southern China, there is a positive trend (0.6–0.9 ppbv yr^{-1}) in surface ozone during the winter season at a coastal site in Hong Kong associated with outflow from mainland China during that season [*Wang et al*., 2009]. These trends in NO_2 and O_3 suggest generally decreasing rates of NO_3 and N_2O_5 production in North America and Europe but a rapidly increasing rate of nighttime chemical reactions in China, with the potential to drive the associated chemical cycles.

Despite its importance to regional air quality and despite the likely rapid increase in the rate of nighttime chemistry, investigations of nighttime nitrogen oxides in China remain relatively sparse. Several studies have identified the role of N_2O_5 uptake in production of aerosol nitrate, a significant component of secondary inorganic aerosol. *Pathak et al*. [2009, 2011] found that heterogeneous N_2O_5 uptake led to accumulation of fine aerosol nitrate downwind of Beijing and Shanghai megacities even under conditions of high aerosol acidity. Recent studies of aerosol loading and composition across China have identified nitrate as an important component (7–14% on average) and have noted the contribution of multiphase chemistry initiated by NO_3 [*Guo et al*., 2014; *Huang et al*., 2014]. A model study of a severe winter haze episode in Beijing showed that inclusion of heterogeneous nitrogen oxide reactions was essential to reproduce observations [*Zheng et al*., 2015]. Similarly, analysis of a winter haze event in Hong Kong with high nitrate loadings showed that N_2O_5 uptake contributed significantly to the nitrate aerosol accumulation rate even during daytime [*Xue et al*., 2014]. Although N_2O_5 production and uptake is a major process underlying aerosol pollution in China, these field studies lack direct measurements of this key intermediate. *Wang et al*. [2013] presented measurements of NO_3 by differential optical absorption spectroscopy, together with NO_2 and N_2O_5 calculated via the equilibrium in reaction (2), within the urban area of Shanghai during August–October 2011. These surface level measurements found NO_3 production rates via reaction (1) of several parts per billion per hour and evidence that sinks for NO_3 and N_2O_5 were dominated by heterogeneous reactions of the latter.

Nighttime reactions of nitrogen oxides are often difficult to characterize in field studies due to the lack of mixing within the planetary boundary layer at night [*Stutz et al*., 2004]. Surface level measurements are representative of either a nocturnal boundary layer, with a depth on the order of 100 m, or a surface layer that may be only tens of meters deep [*Stull*, 1988]. Measurements at the surface do not characterize the composition or chemistry of the much deeper residual layer, where the largest mass from the previous day's emission resides. Strategies for probing the residual layer include measurements from aircraft [*Brown et al*., 2007; *Kennedy et al*., 2011], tall towers [*Benton et al*., 2010; *Wagner et al*., 2013], or terrain features that lie within the residual layer [*Crowley et al*., 2010].

Here we present measurements of nighttime nitrogen oxides and related species from Tai Mo Shan, a coastal mountaintop site in Hong Kong, China, with an elevation of 957 m. Measurements took place during November and December 2013, during the latter part of the season with high ozone pollution in Hong Kong [*Wang et al*., 2009]. The Tai Mo Shan campaign included measurements of NO_3, N_2O_5, $ClNO_2$, HONO, O_3, VOCs, particle size distributions, and aerosol ionic composition. The study provides a comprehensive

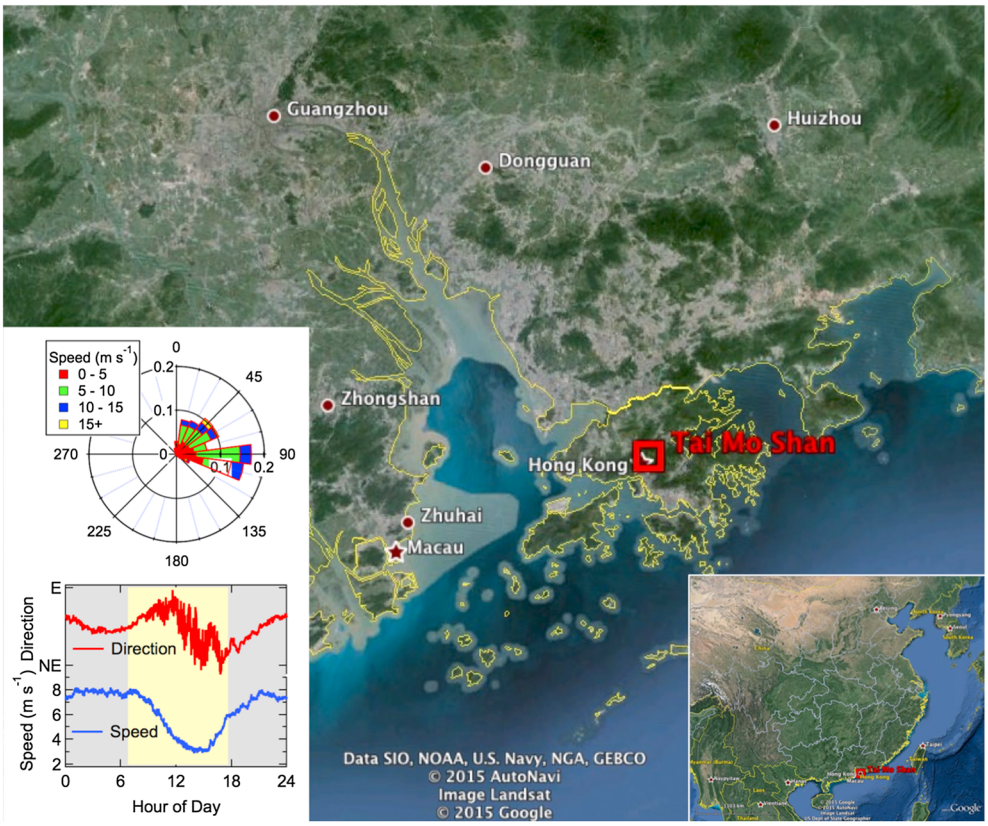

Figure 1. Map of the Pearl River Delta area of southeast China showing the location of the Tai Mo Shan mountaintop observatory. The left inset shows a wind rose (top) and the diurnal average wind direction and wind speed during the study period (bottom). Winds were exclusively from the east and northeast and most commonly between 5 and 10 m s^{-1}. Nighttime and early morning winds were strong, while late afternoon winds were slack. The average direction rotated slightly to the northeast in the afternoon during the period of slower average wind speed.

analysis of nighttime chemistry in an Asian megacity and the first observations of nighttime chemistry within the residual layer in Asia. This paper examines the nighttime chemistry of NO_3 and N_2O_5, while a companion paper [*Wang et al.*, 2016] describes observations and analysis of nitryl chloride, $ClNO_2$.

2. Field Site and Instruments

The Tai Mo Shan observatory is located north of major population centers of Hong Kong (Kowloon and Hong Kong) and to the south of Shenzhen in mainland China (Figure 1). It is the highest point in Hong Kong at 957 m. This altitude is near the top of the average daytime mixed layer height in Hong Kong during autumn (1.2 km) and winter (1.0 km)[*Yang et al.*, 2013]. Thus, during the November–December study period, the site would lie near the top of the residual layer at night, with the potential to sample from the free troposphere at times. Although the site was high enough to encounter clouds and was thus frequently impacted by fog during the study period (see below), measured levels of pollutants were nearly always characteristic of at least a moderately polluted boundary layer. Median (average) total reactive nitrogen, NO_y, was 6.15 ppbv (7.88 ppbv), with an interquartile range (25th–75th percentiles) of 4.51–9.13 ppbv and a 10th–90th percentile range of 3.14–13.98 ppbv. Thus, regardless of whether the sampled air was influenced more by the boundary layer or free troposphere, it was always impacted by regional pollution. All instruments were housed in a small, custom-built shelter with inlets affixed to a scaffold above the shelter roof at a height of 6 m above ground level at the mountaintop site.

A companion paper on $ClNO_2$ observations during this campaign [*Wang et al.*, 2016] gives a detailed description of the instrumentation for trace gas, aerosol, radiation, and meteorological measurements. The focus of the current paper is on the analysis of NO_3 and N_2O_5. Briefly, these species were measured using diode laser

cavity ring-down spectroscopy (CRDS) at 662 nm [*Wagner et al*., 2011]. The instrument measures NO_3 directly by optical extinction on its strong, 662 nm absorption band. It measures the sum of NO_3 and N_2O_5 simultaneously in a separate channel through a heated inlet that thermally dissociates N_2O_5 to NO_3. Precision and accuracy for N_2O_5 are ≤3 parts per thousand by volume (pptv) (2σ, 1 s) [*Wagner et al*., 2011] and ±12% [*Fuchs et al*., 2008], respectively. The stated precision and accuracy for NO_3 is normally approximately equivalent to that of N_2O_5. However, for the data from this campaign, NO_3 was observed to be substantially lower (60%) than the mixing ratio predicted by the NO_3-N_2O_5 equilibrium in reaction (2), contrary to experience with previous airborne and ground-based measurements with this technique [*Brown et al*., 2003b; *Osthoff et al*., 2007], indicating a large loss for this species in the instrument inlet during this campaign. The reported NO_3 was corrected for this loss factor based on its predicted ratio to N_2O_5. Because of the much larger associated uncertainty in NO_3 for this campaign, and because the resulting NO_3 measurement is not independent of N_2O_5, the analysis reported in this paper relies on the N_2O_5 measurement only. The inlet was constructed of 6 m of 1/4 inch (6.35 mm) OD, 5/32 inch (4.0 mm) ID fluorinated ethylene propylene Teflon tubing, with a restriction at the end of the inlet that dropped the pressure below 300 mbar. The total volumetric flow in the inlet was approximately 20 L/min, for a residence time of 0.2 s. It is not clear whether the NO_3 loss occurred in this inlet, the filter housing (residence time 0.06 s), or the tubing used to construct the sample cells around the optical detection axis (residence time 0.25 s). Periodic exchanges of the external inlet tubing did not change the apparent NO_3 transmission. Transmission of N_2O_5 is generally much greater than that of NO_3 [*Fuchs et al*., 2008], and comparison between the CRDS N_2O_5 and a measurement based on chemical ionization mass spectrometry showed excellent agreement [*Wang et al*., 2016]. Thus, the N_2O_5 measurement is taken here as correct, while the NO_3 measurement is assumed to suffer from inlet losses during this campaign. Transmission of N_2O_5 has been found independent of relative humidity (RH) up to 95% [*Fuchs et al*., 2008]. However, potential inlet N_2O_5 loss at 100% RH (i.e., fog) is unknown. Section 5 discusses N_2O_5 measurement in polluted, daytime fog, where small but nonzero N_2O_5 was observed and taken to be accurate.

The same instrument also measures NO, NO_2, NO_y, and O_3 by diode laser CRDS at 405 nm. In this case, NO_2 is measured directly by optical extinction, and NO, O_3, and NO_y are converted quantitatively to NO_2 in three additional, separate measurement channels. Measurement precision is equal to or better than 60 pptv (2σ, 1 s), and the accuracy is 3% for NO_2 and O_3, 5% for NO, and 12% for NO_y. Linear fits using orthogonal distance regressions of NO_2, NO, and NO_y measured by CRDS against measurements from a chemiluminescence analyzer showed slopes of 0.97 ± 0.01, 0.91 ± 0.01, and 1.11 ± 0.01, respectively (errors are 2σ fit errors). Comparison of CRDS O_3 to a commercial 254 nm UV absorption instrument showed a slope of 1.00. The CRDS measurements operated from 15 November to 6 December 2013, while the chemiluminescence NO_x, NO_y, and UV absorption O_3 operated through 14 December. Data analyzed in this manuscript use CRDS NO_2, NO_y, and O_3 but use the other instruments to fill in data gaps in the CRDS instrument, including the entire period after 6 December.

As described in the companion paper [*Wang et al*., 2016], $ClNO_2$ was measured by iodide ion chemical ionization mass spectrometry with a precision of 4 pptv (2σ, 1 min) and an accuracy of 20%.

3. Measurement Overview

The local airflow at Tai Mo Shan was exclusively from the east and northeast as the wind rose in Figure 1 shows. This direction was mainly onshore from the South China Sea and occasionally parallel to the coastline or slightly offshore from mainland China. During the night and early morning, winds were consistently stronger and more easterly (onshore), with an average wind speed of 8 m s^{-1}. During late morning through late afternoon the average wind speed gradually slackened to 3 m s^{-1} by 15:00. A slight rotation of the average wind direction toward the northeast, and slightly more from mainland China, accompanied the afternoon wind slackening. Most individual days had slower afternoon wind speeds, but fewer days exhibited the local wind direction shift. Despite a local wind direction from the South China Sea, air masses were never observed to be free of pollution, indicating the importance of mixing between continental outflow and the prevailing easterly flow, as described in more detail in the companion paper [*Wang et al*., 2016]. Figure 2 shows a series of backward trajectory calculations using the Hybrid Single-Particle Lagrangian Integrated Trajectory (HYSPLIT) model [*Draxler and Rolph*, 2003] and covering the majority of the study

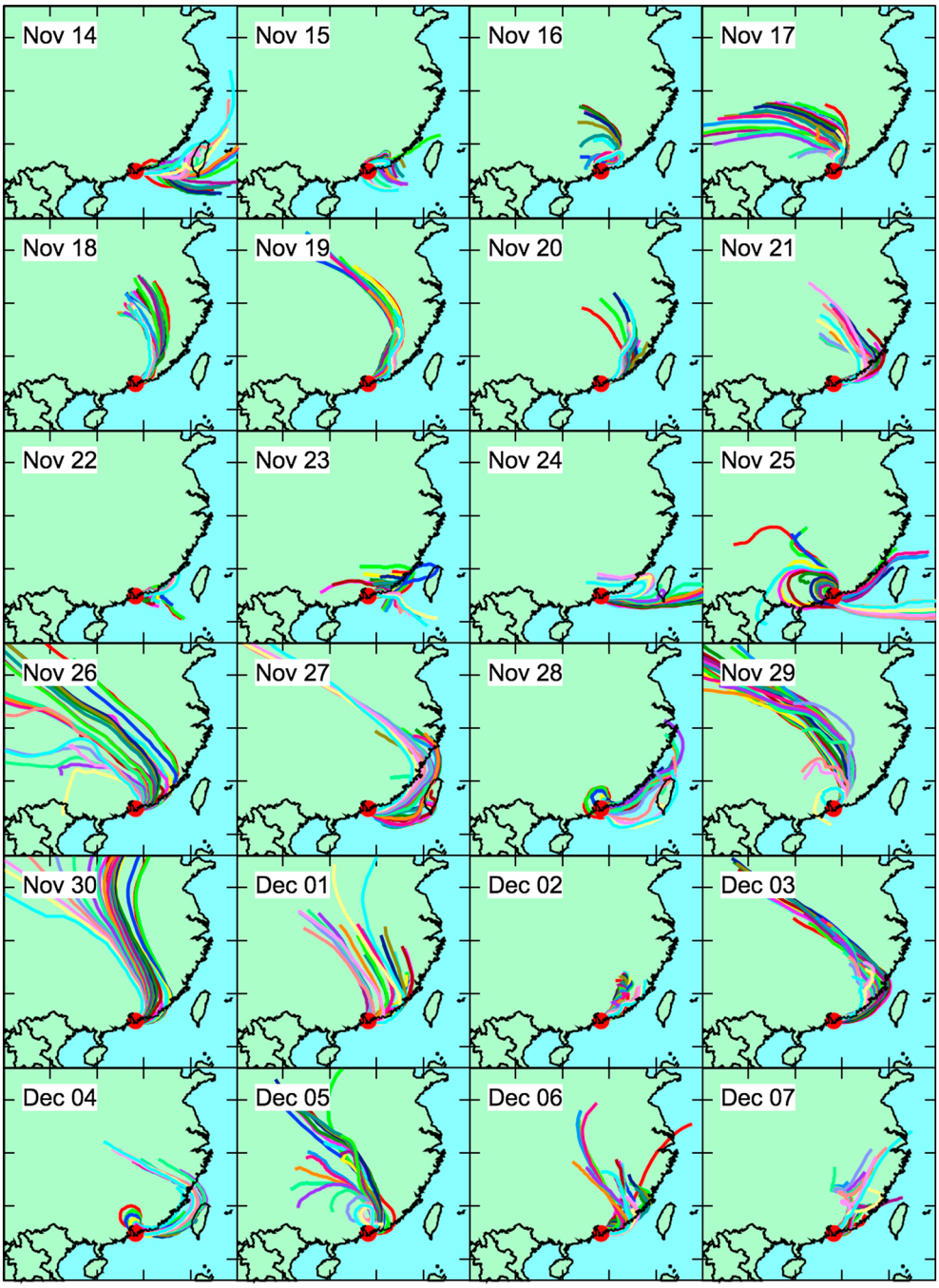

Figure 2. Backward trajectory calculations using the HYSPLIT model during the study period. Trajectories are 48 h in duration, initialized every hour at observatory location and 1 km altitude. Trajectories begin at 0Z (8 A.M. local) on the date shown.

period, from 14 November to 7 December 2013. The trajectories are consistent with arrival of air masses from the north and east of the site, but they also clearly show the passage of most air masses over mainland China or Taiwan throughout much of the 48 h of transport on many of the measurement days. The only exceptions are 24–25 November and part of 27 November, when the longer range airflow was distinctly from the east. On these occasions, air at the site had lower O_3, higher NO_x, and a higher NO_x to NO_y ratio (see below), consistent with entrainment of strong local NO_x emissions from the city of Hong Kong into air with lower O_3 transported inward from the South China Sea.

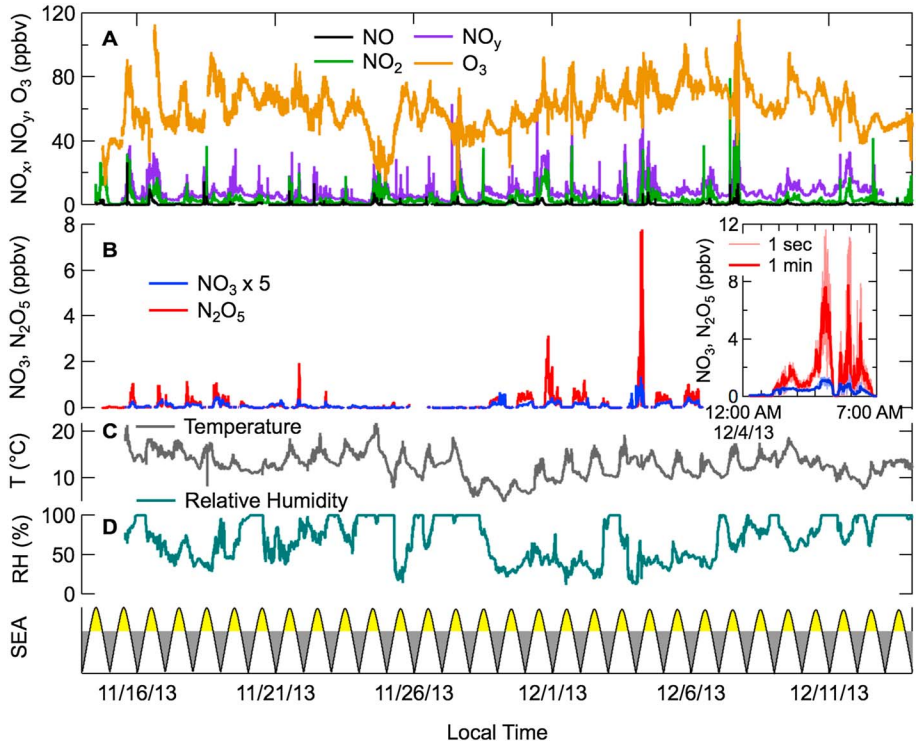

Figure 3. Time series of (a) NO, NO_2, NO_y and O_3; (b) NO_3 and N_2O_5; (c) temperature; and (d) relative humidity. The bottom plot shows solar elevation angle to reference night and day. Data are at 1 min time resolution. The inset in Figure 3b shows 1 min and 1 s data for the time period from midnight to 7 A.M. on 4 December, when N_2O_5 reached its maximum concentration.

The time series of nitrogen oxides and ozone in Figure 3 is consistent with the picture of regionally polluted air at the mountaintop site. Nitrogen oxides (NO_x) and total reactive nitrogen (NO_y) were variable, as noted above, with a wide range of NO_x/NO_y ratio, indicating a wide range of air mass age sampled at the site. Ozone exhibited characteristic afternoon photochemical peaks, exceeding 80 ppbv in the afternoon on 15 out of 31 days and exceeding 100 ppbv on three days. The nighttime nitrogen oxides, NO_3 and N_2O_5, were similarly variable. Nightly maximum N_2O_5 was in excess of 0.5 ppbv on every night that was not impacted by fog. However, fog was a persistent feature of the site, as shown by the relative humidity time series in Figure 3. Relative humidity (RH) reached 100% for part or all of 16 nights during the entire 31 day study and on 9 of the 21 nights during which N_2O_5 was measured with the CRDS instrument. Measured N_2O_5 was much lower on foggy nights, especially the period from 22 to 28 November when nightly N_2O_5 was nearly always below 0.2 ppbv and frequently below 10 pptv. Levels of NO_x were similar on foggy and nonfoggy nights, suggesting that the lower N_2O_5 was due to its rapid loss to heterogeneous uptake in fog droplets.

3.1. Diel Averages

Figure 4 shows diel average data for NO_x, NO_y, and O_3. Total reactive nitrogen (NO_y) was at its lowest average value between midnight and sunrise (6:47 A.M. campaign average) at 5.8 ppbv but increased steadily throughout the day to a maximum average value of 13.2 ppbv between 16:00 and 17:00. In terms of nitrogen oxidation, air was also most aged between midnight and sunrise, with average NO_x/NO_y of 0.29 ± 0.03 (1σ). The average NO_x/NO_y ratio decreased continuously through the night at a rate of $0.014\,h^{-1}$. The NO_x/NO_y ratio increased during daytime, with the maximum NO_x/NO_y occurring between noon and sunset and an average NO_x/NO_y of 0.41 ± 0.03 during daylight hours. The steady rise in NO_x and NO_y throughout the day, together with the increase in the NO_x/NO_y ratio, indicates less aged air sampled at the mountaintop site during daytime, when the boundary layer is presumably well mixed relative to nighttime. At night, the site is likely more isolated from surface emissions.

At the average late night O_3 (58 ppbv) and temperature (285 K), the lifetime of NO_x with respect to oxidation via reaction (1) is 4.5–9.0 h, with the longer lifetime corresponding to $1 \times k_1[O_3]$ (where k_1 is the rate

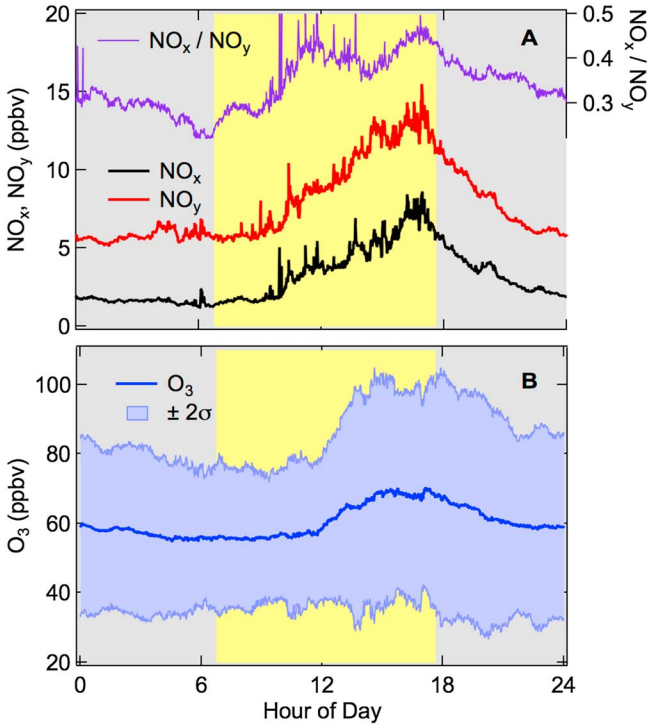

Figure 4. Diel average data. (a) NO_x, NO_y (left axis), and their ratio, NO_x/NO_y (right axis); (b) O_3, with shaded area showing 2σ variation. Grey and yellow shading on the background indicates the average period of darkness and sunlight, respectively.

coefficient for reaction (1)) and representing the case where NO_3 and N_2O_5 react mainly through NO_3. The shorter lifetime corresponds to $2 \times k_1[O_3]$ and represents reactions mainly through N_2O_5 [*Brown et al.*, 2004]. These calculations presume reaction of NO_3 with NO to be negligible, which is reasonable for chemistry occurring in the residual layer well removed from direct NO emissions. In the absence of NO_y loss to dry deposition, the average late night NO_x/NO_y ratio is equivalent to an aging time by dark chemistry of 5.5–11 h, i.e., comparable to the duration of a single night. The average nighttime NO_x/NO_y decay rate is, however, considerably slower than that from reaction (1), likely due to averaging of air masses of different photochemical and dark chemistry ages. Comparison of nighttime to daytime oxidation rates requires an estimate of OH radical concentrations, which were not measured or easily constrained by other measurements at this site. For an average daytime OH of $2–5 \times 10^6$, the photochemical lifetime of NO_2 would be in the range 5.5–14 h if OH radical reaction with NO_2 were the dominant NO_x sink and shorter if other sinks ($NO + RO_2$, PAN formation) were significant [e.g., *Day et al.*, 2003]. The estimated photochemical NO_x lifetime range is comparable to the nocturnal lifetime range.

The diurnal pattern of O_3 was typical of that for urban-influenced environments, with a late afternoon maximum of 68.5 ppbv and daily average rise of 12 ppbv. Average O_3 did not begin to increase until late morning, with the entire average increase occurring between 11:00 and 15:00. The apparently late onset of O_3 photochemistry may indicate that the boundary layer growth containing emissions from the surrounding urban areas does not reach the site until approximately 11 A.M. at this time of year.

3.2. High-Concentration, Variable Urban Plumes Sampled at Night

As discussed above, Tai Mo Shan is generally influenced by polluted onshore flow that periodically mixes with continental outflow. A few high-concentration urban plumes whose likely origin was the megacities of the Pearl River Delta region impacted the site at night during discrete events. During these periods, nitrate radical production rates varied from a few tenths to a few ppbv h^{-1}, and N_2O_5 exhibited periodic large variability (see next paragraph) that was apparent only in data recorded at high time resolution. These characteristics appear to be consistent with infrequent nighttime intercepts of intense pollution plumes at Tai Mo Shan, which is adjacent to but generally not directly downwind of the large megacities of the Pearl River Delta area. High concentrations and large variability may also arise from sampling from a residual layer air mass that has vertically stratified plumes with large spatial gradients [e.g., *Brown et al.*, 2007].

All data in Figure 3 are shown at a time resolution of 1 min except for the inset, which shows the period from midnight to 7 A.M. on 4 December at 1 s resolution. This event had by far the largest N_2O_5 concentrations observed during the campaign as well as the largest variability in N_2O_5. This maximum N_2O_5 is the largest directly measured concentration reported in the literature to date and comparable to N_2O_5 levels inferred from measurements of NO_3 radicals in the Los Angeles Basin in the late 1970s [*Atkinson et al.*, 1986]. One-minute average N_2O_5 exhibited three distinct maxima of 7.7, 7.8, and 5.2 ppbv. During the first two

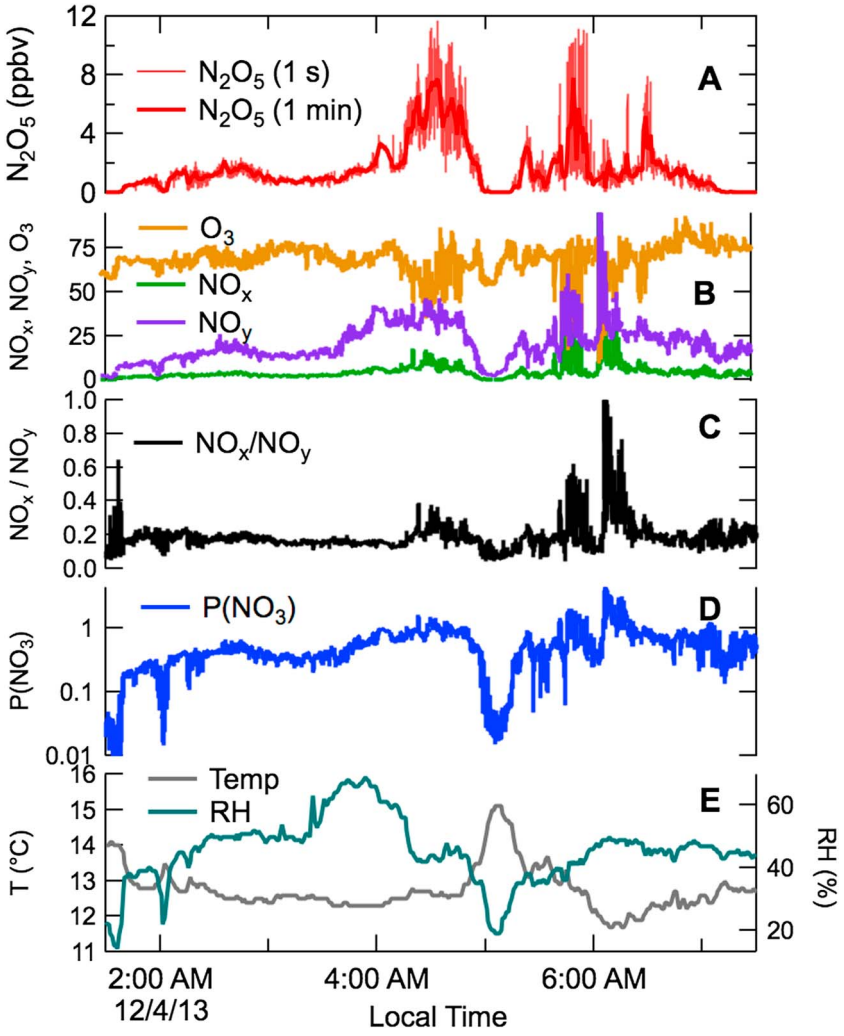

Figure 5. Expanded view from 1:30 to 7:30 on 4 December of the time series for (a) N_2O_5 at 1 s and 1 min resolution; (b) O_3, NO_x, and NO_y in ppbv at 1 s resolution; (c, d) NO_x/NO_y and nitrate radical production rate, $P(NO_3)$ in ppbv h^{-1}, respectively, at 1 s; and (e) temperature and relative humidity at 1 min.

maxima, 1 s N_2O_5 had a standard deviation of 1.5 and 2.7 ppbv, respectively, with relative standard deviations (standard deviation divided by the average) of 19% and 35%. The N_2O_5 in the 1 s data reached a maximum mixing ratio of 11.7 ppbv (The CRDS instrument's dynamic range is estimated to be linear up to approximately 100 ppbv).

Variability in the N_2O_5 concentrations at the Tai Mo Shan station was accompanied by large variability in NO_x and in air mass age. Figure 5 shows an expanded view of N_2O_5, NO_x, NO_y, O_3, the NO_x to NO_y ratio, and the nitrate radical production rate at 1 s time resolution for 1:30–7:30 A.M. on 4 December. Also shown is RH and temperature at 1 min, the best available time resolution for these data. Although the wind was steady from the east (97 ± 3°) with a relatively high wind speed (12.9 ± 0.7 m s^{-1}) during the entire period, NO_3, N_2O_5, NO_x, and NO_y varied considerably. Prior to 1:30 A.M. and for a short period just after 5 A.M., temperature was slightly higher and relative humidity considerably lower. The NO_x was low and the air was relatively more aged, with $NO_x/NO_y \sim 0.1$; the production rate of nitrate radicals from reaction (1), $P(NO_3) = k_1[O_3][NO_2]$, was well under 0.1 ppbv h^{-1}, approaching 0.01 ppbv h^{-1}. These characteristics are consistent with highly aged, polluted air, in which NO_x had been nearly completely oxidized, sampled from above the residual layer. Slightly lower temperature and increased RH after 1:45 A.M. brought $NO_x/NO_y \sim 0.2$ and $P(NO_3)$ of several hundred pptv h^{-1}, consistent with a moderately polluted residual layer and moderate nighttime chemistry. Higher NO_x/NO_y, increased $P(NO_3)$, and much higher variability in N_2O_5 characterized the three large maxima

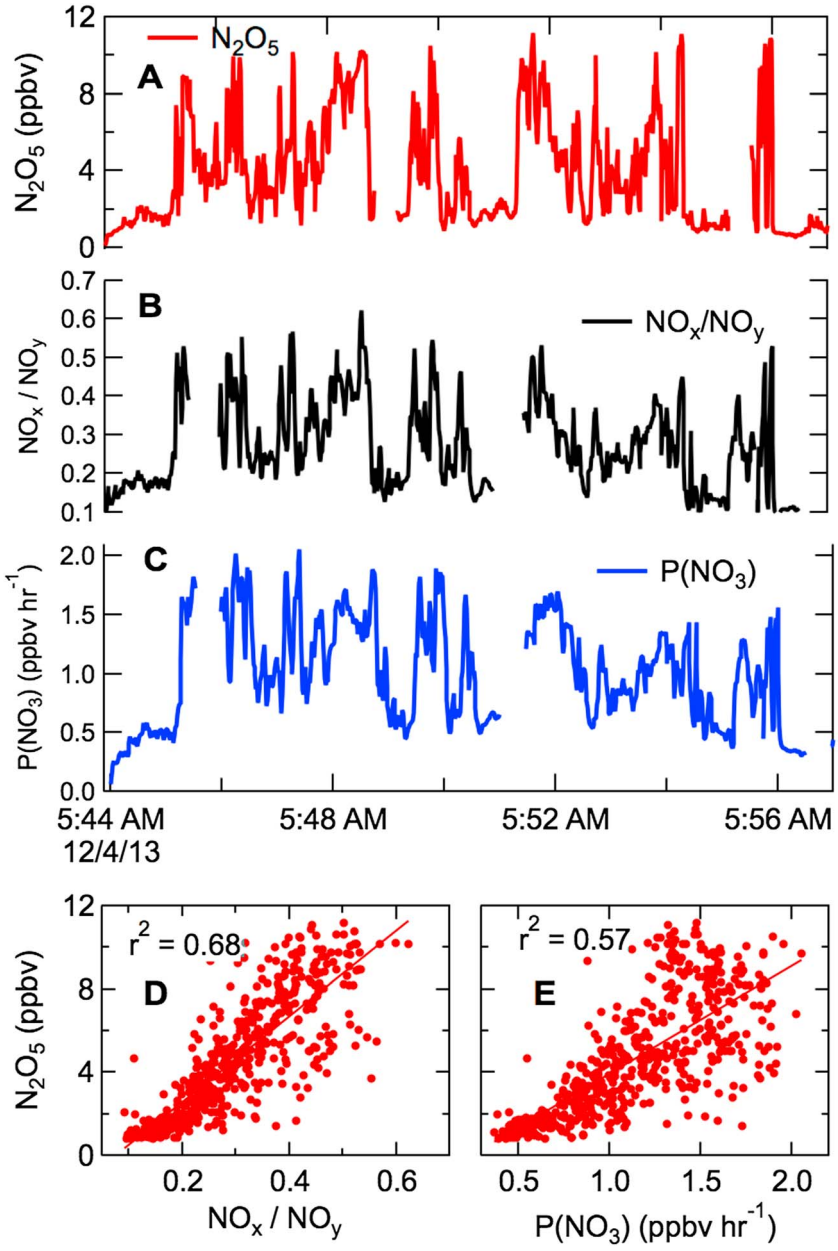

Figure 6. Expanded view of the second large N_2O_5 plume near 5:45 A.M. from Figure 4 showing (a) N_2O_5; (b) NO_x/NO_y; (c) $P(NO_3)$; and (d, e) correlations of N_2O_5 with NO_x/NO_y and $P(NO_3)$.

in N_2O_5 near 4:30, 5:45, and 6:30 A.M. The large increase in NO_x/NO_y and $P(NO_3)$ near 6:15 A.M. did not follow the same pattern and was not accompanied by large N_2O_5 but also had NO_x/NO_y near 1, indicative of much more recently emitted NO_x pollution.

Figure 6 illustrates the characteristics of the 5:45 A.M. plume that showed the highest concentrations and the greatest variability in N_2O_5. Variabilities in NO_x/NO_y (0.1–0.5) and $P(NO_3)$ (0.5–2.0 ppbv h^{-1}) were large and well correlated with variability in N_2O_5, indicating that variability in the latter was the result of a rapid shift between NO_x-rich and NO_x-poor air masses. The correlation of N_2O_5 with NO_x/NO_y was slightly better than with $P(NO_3)$, though both were comparable. Sampling of different air masses on a rapid time scale from a mountaintop site could occur if the air pollution plume were confined to a maximum altitude range just equal to the site elevation or if it were transported in a narrow vertical layer. Narrow, vertically layered plumes have been observed, for example, from aircraft measurements of emissions from coal-fired electric power

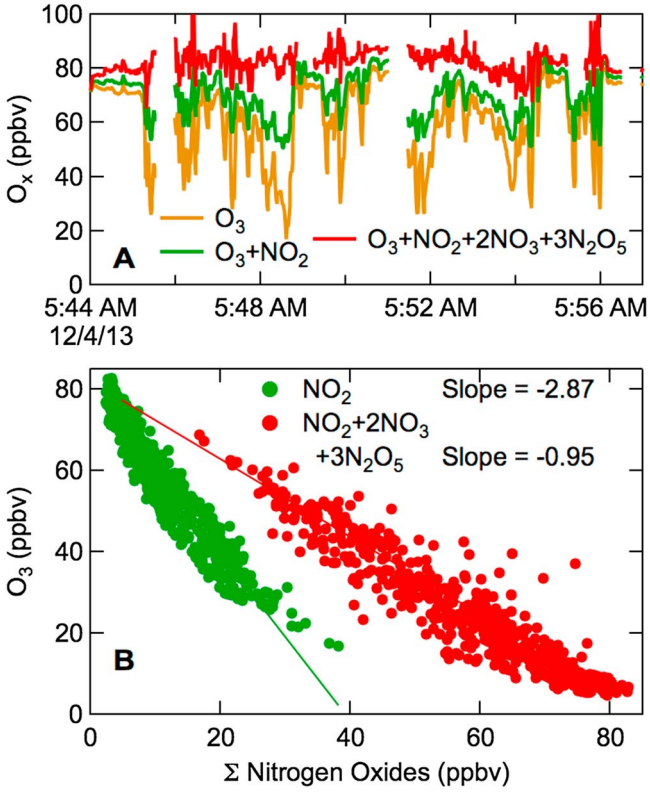

Figure 7. Odd oxygen budget for the 5:45 A.M. plume from Figures 4 and 5. (a) Time series of O_3, $O_x = O_3 + NO_2$, and nighttime $O_x = O_3 + NO_2 + 2 \times NO_3 + 3 \times N_2O_5$; (b) plots of O_3 against NO_2 and $NO_2 + 2 \times NO_3 + 3 \times N_2O_5$. The slope of the first plot is a measure of plume age (5.4–7.4 h), while the slope of the second plot is a measure of nighttime O_x conservation (slope near −1 indicates conservation of nighttime O_x in the N_2O_5 reservoir).

generation plants in the residual layer [*Brown et al.*, 2007]. The large variability in N_2O_5 is similar to that observed previously in Boulder, CO, USA, from a mesa site located on a terrain feature above an urban area [*Brown et al.*, 2003b], similar to Tai Mo Shan but at much lower elevation relative to the nearby urban area. At the Boulder site, variability was shown to arise from large loss rates for NO_3 and N_2O_5, since the corresponding variability in NO_2 and O_3, the source gases for NO_3 and N_2O_5, was small.

As shown in the companion paper [*Wang et al.*, 2016], the highly polluted air mass observed on the night of 4 December came from the Pearl River Delta region based on back trajectories that were calculated with high-resolution wind data simulated by a mesoscale model. Tai Mo Shan, situated to the southeast of Guangzhou and Shenzhen, encounters these plumes infrequently at night, and the large variability may be indicative of the unusual mixing that brings such plumes to this site. Sites situated farther to the west of Tai Mo Shan may encounter large urban plumes during nighttime with greater frequency. Although they are infrequent occurrences at Tai Mo Shan, these intense urban plumes may in fact be characteristic of the nighttime outflow from the Pearl River Delta megacities.

3.3. Nocturnal Odd Oxygen

The observation of a large pollution plume exhibiting rapid variability between background and polluted air provides an opportunity to analyze its nocturnal odd oxygen budget. The conventional definition of tropospheric odd oxygen, O_x, is the sum of NO_2 and O_3, since these species rapidly interconvert photochemically. Nocturnal odd oxygen also includes NO_3 and N_2O_5 in their stoichiometric ratio with the number of O_3 molecules required to form each compound through reactions (1) and (2) [*Brown et al.*, 2006a].

$$O_x = NO_2 + O_3 \quad (6)$$

$$\text{Nocturnal } O_x = NO_2 + O_3 + 2NO_3 + 3N_2O_5 \quad (7)$$

Figure 7a shows O_3, O_x, and nocturnal O_x for the 4 December 5:45 A.M. plume. Whereas O_3 and O_x show large variability, similar to that seen in N_2O_5, NO_x/NO_y, and $P(NO_3)$, nocturnal O_x is approximately constant across the entire plume intercept. This behavior indicates a nighttime emitted plume that did not undergo photochemical O_3 production but rather only O_3 consuming reactions during darkness. Figure 7b shows a plot of O_3 against NO_2 and against the sum of nitrogen oxides in their stoichiometric ratio to O_3, i.e., $NO_2 + 2NO_3 + 3N_2O_5$. Ozone and NO_2 are tightly anticorrelated. If the majority of the NO_x emissions had occurred in the form of NO (i.e., little primary NO_2), a fit of O_3 against NO_2 should yield a slope close to −1 if no nighttime NO_2 oxidation had occurred. Slopes steeper than this value indicate the further nighttime oxidation of NO_2. This nocturnal relationship between O_3 and NO_2 is a chemical clock defined by the rate coefficient for reaction (1) with an analytically simple, linear expression that is accurate as long as O_3 is in excess of NO_2

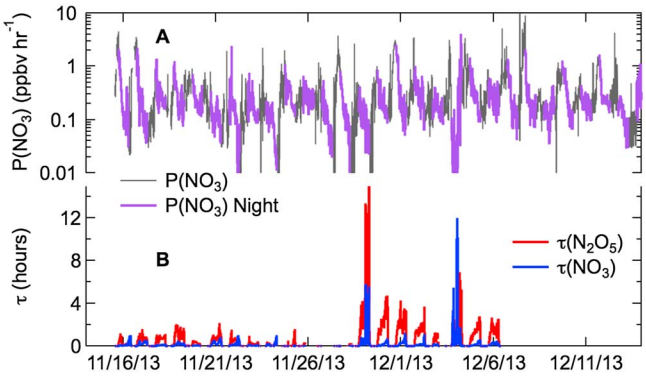

Figure 8. Time series of (a) NO_3 production rate, with heavier purple overlay indicating nighttime data and (b) N_2O_5 and NO_3 lifetimes.

[*Brown et al.*, 2006a]. To satisfy this condition, the fit is only for the initial portion of the O_3 versus NO_2 plot between 60 and 80 ppbv, yielding a slope of −2.87. Conversion of this slope to a processing time depends on the fate of NO_3 and N_2O_5 (i.e., loss through NO_3, loss through N_2O_5, or a stable reservoir) but gives a range of 5.4–7.4 h. Although the local wind speed and direction indicated steady transport from the east or northeast, the high-resolution transport analysis in the companion paper [*Wang et al.*, 2016] indicates that the urban pollution in this plume originated in the Pearl River Delta area of mainland China. Because the prevailing wind at this site normally did not pass over the urban areas of this region, intercepts of pollution from this region were infrequent. However, it is likely that the urban plumes from the Pearl River Delta undergo significant nighttime chemistry within the residual layer with substantial mixing ratios of both N_2O_5 and $ClNO_2$.

The constant O_x in Figure 7a and the slope near −1 for O_3 versus $NO_2 + 2NO_3 + 3N_2O_5$ in Figure 7b indicates that most of the odd oxygen consumed through reactions (1) and (2) is conserved in the form of a stable reservoir of N_2O_5, assuming that there is no influence of surface level NO emissions during transport within the residual layer at the sampled altitude during the night. Uptake of N_2O_5 evidently was relatively slow in this plume, whose relative humidity was 42%.

4. Reactivity and Lifetimes of NO_3 and N_2O_5

Both NO_3 and N_2O_5 are reactive intermediates that undergo reactions with volatile organic compounds and heterogeneous uptake to aerosol, respectively. The relative rates of these sink reactions are important to understanding the principal reaction products from nighttime chemistry and their influence on reactive nitrogen, ozone, and aerosols. The steady state lifetimes of NO_3 and N_2O_5, $\tau(NO_3)$, and $\tau(N_2O_5)$, are the ratio of their observed mixing ratios to the nitrate radical production rate, $P(NO_3)$, and are commonly used measures of their reactivity [*Brown et al.*, 2003a; *Platt et al.*, 1984].

$$\tau(NO_3) = \frac{NO_3}{k_1 O_3 NO_2}; \quad \tau(N_2O_5) = \frac{N_2O_5}{k_1 O_3 NO_2} \tag{8}$$

Figure 8 shows the time series of $P(NO_3)$ (log scale), $\tau(NO_3)$, and $\tau(N_2O_5)$. Nitrate radical production rates (1 min averages) varied over more than 3 orders of magnitude, from less than 0.01 ppbv h^{-1} to 10 ppbv h^{-1}, with an average value of 0.32 ppbv h^{-1}. Nitrate radical production rates tended to peak in late afternoon, concurrently with the maximum in NO_x and O_3, and then decrease slowly during the night. Thus, the most active period for nighttime chemistry, at least in terms of radical production rates, was during early evening just after sunset. Nighttime average $P(NO_3)$ was slightly lower, at 0.26 ppbv h^{-1}. Lifetimes of NO_3 and N_2O_5 varied from <0.1 to 13 h, although the very long lifetime events corresponded to low production rates and small denominators in equation (8) rather than large mixing ratios of NO_3 and N_2O_5. Under more polluted conditions typical of the majority of the data, nightly maximum N_2O_5 lifetimes varied over the range 1–2 h during the first half of the campaign (15–26 November) and 2–5 h in the second half (28 November to 6 December). Relative humidity was higher during the first period (73 ± 22%) than during the second (45 ± 19%). The N_2O_5 lifetime showed a clear dependence on relative humidity (Figure 9), consistent with its heterogeneous uptake in reactions (4) and (5) playing a large role as a sink reaction. Its lifetime varied from a median above 2 h at 25% RH to 0.3 h at 95% RH. A part of this difference may be due to increased aerosol surface area due to hygroscopic aerosol growth at higher RH, and a part may be due to an RH dependence of the N_2O_5 uptake coefficient [*Brown and Stutz*, 2012]. Figure 9b shows the dependence of $\tau(N_2O_5)$ on aerosol surface area, which includes hygroscopic growth. The lifetime decreases with

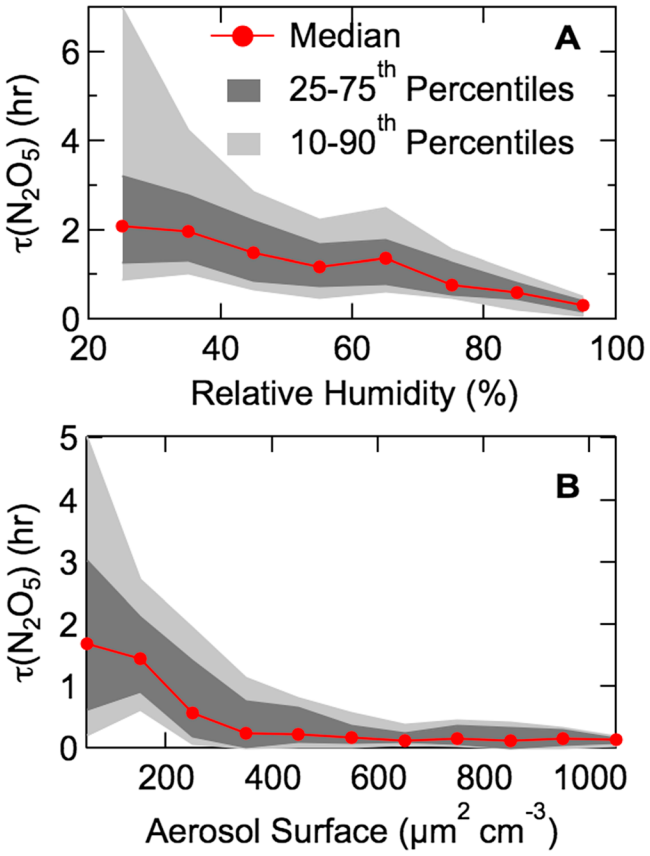

Figure 9. N_2O_5 lifetime from 3 h past sunset until sunrise versus (a) relative humidity, binned in increments of 10% and (b) aerosol surface area, binned in increments of 100 μm^2 cm^{-3}. Data are shown as medians, 25–75th percentile ranges, and 10–90th percentile ranges, as shown in the legend.

increasing surface area up to 500 μm cm^{-3} but is approximately constant thereafter. The large majority (85%) of the data occurred at surface areas smaller than this threshold, however. The trend in $\tau(N_2O_5)$ with aerosol surface area may arise either from increased N_2O_5 uptake rates at higher available surface area or with increased rates of NO_3-VOC reactions in more polluted air with larger aerosol loads.

4.1. Individual Sinks for NO_3 and N_2O_5

Because NO_3 and N_2O_5 are in rapid thermal equilibrium, the individual sinks for either compound contribute to the removal of the pair. The dependence of the steady state lifetime on NO_2, which determines the ratio of NO_3 and N_2O_5 and thus the relative importance of the reactions of either to the loss of the pair, is one method for separating the individual contributions of NO_3 reactions and N_2O_5 heterogeneous uptake [*Brown et al.*, 2003a]. This method has been demonstrated for sampling within the residual layer during transects of individual NO_x plumes sampled aloft from aircraft [*Brown et al.*, 2006b; *Brown et al.*, 2009]. A linear form of this relationship that gives the N_2O_5 uptake coefficient, $\gamma(N_2O_5)$ as the slope, and the first-order loss rate coefficient for NO_3, $k(NO_3)$ as the intercept, is as follows [*Brown et al.*, 2009].

$$\tau(N_2O_5)^{-1}K_{eq}[NO_2] = k(NO_3) + \frac{1}{4}cS_AK_{eq}[NO_2]\gamma(N_2O_5) \quad (9)$$

Here K_{eq} is the temperature-dependent equilibrium coefficient for the NO_3-N_2O_5 equilibrium in reaction (2), c is the mean molecular speed of N_2O_5, and S_A is the aerosol surface area. Figure 10 shows an example plot of $\tau(N_2O_5)^{-1}K_{eq}[NO_2]$ versus $\frac{1}{4}cS_AK_{eq}[NO_2]$ for 20–21 November. Although an equation similar to (9) can be written for $\tau(NO_3)$, the NO_3 measurement was not independent of N_2O_5 for this data set, and only the N_2O_5 plot is shown. Equation (9) is approximately valid if NO_3 and N_2O_5 have achieved steady state, i.e., if dNO_3/dt and dN_2O_5/dt are both approximately 0. Steady state lifetimes increased continuously on many nights during approximately the first 3 h after sunset, indicating an approach to steady state of approximately this duration. Data in Figure 10 and for determinations from other nights therefore exclude the first 3 h of data. Previous analysis of aircraft measurements in other locations has shown that S_A exhibits a positive, linear correlation with NO_2 and that this covariance can be accounted for by explicit inclusion of S_A in equation (9) [*Brown et al.*, 2009]. Covariance may also occur between NO_2 and $k(NO_3)$. A positive covariance between these quantities would increase the slope and decrease the intercept of the linear fit, leading to an overestimate of $\gamma(N_2O_5)$ and an underestimate of $k(NO_3)$. Indeed, fits to the data on several nights produced negative values for $k(NO_3)$, potentially as a result of this covariance. Table 1 shows $\gamma(N_2O_5)$ and $k(NO_3)$ derived from similar fits to 10 nights of the campaign. Nights with negative $k(NO_3)$ were excluded. Data were also filtered for RH $<$ 90% due to the uncertainty in the aerosol surface area at high RH [*Wang et al.*, 2016]. Averaged across all nights on which the determination was possible, $\gamma(N_2O_5) = 0.014 \pm 0.007$ and $k(NO_3) = 5.6 \pm 2.5 \times 10^{-4}$ s^{-1}.

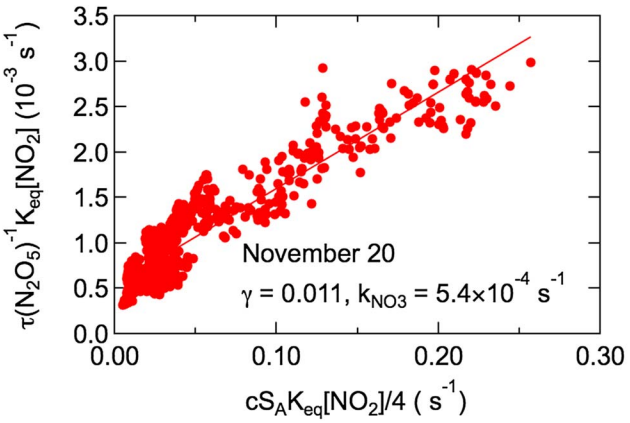

Figure 10. Example fit of N_2O_5 lifetime according to equation (9) for data from the night of 20–21 November.

Because of the potential covariance described above, these values are simply the best fits for $\gamma(N_2O_5)$ and $k(NO_3)$ to within these limitations. They do not account for potential variability in these quantities but do represent the average values of these parameters that best describe the steady state lifetimes of the observed data. The derived $\gamma(N_2O_5)$ lie within the range of 0.002–0.04 from previous field-based determinations from aircraft or tall tower sampling in the residual layer, which generally range from 0.001 to 0.04 [*Brown et al.*, 2006b, 2009; *Wagner et al.*, 2013]. The $k(NO_3)$ are low, corresponding to a nighttime NO_3 lifetime in excess of 30 min. Low average NO_3 reactivity is consistent with measurement in relatively aged air within the residual layer depleted in reactive VOCs.

Figure 11 shows a diel average of $\tau(N_2O_5)$ from equation (8) (black line) for all data with RH < 90%. (The large plumes of N_2O_5 do not exhibit lifetimes that are as much larger as the N_2O_5 mixing ratios themselves and thus do not bias the diel averaged lifetime.) Also shown on the plot is the calculated N_2O_5 lifetime for three cases. Calculated lifetimes are derived from equation (9) as follows.

$$\tau(N_2O_5)_{Calc} = \left[\frac{k(NO_3)}{K_{eq}[NO_2]} + \frac{1}{4}cS_A\gamma(N_2O_5)\right]^{-1} \quad (10)$$

Calculated lifetimes are shown continuously throughout the diel cycle but are only comparable to the observations at night. Case 1 (green line) represents all reactivity of NO_3 and N_2O_5 attributed to N_2O_5 uptake. In this case, the uptake coefficient that best matches the data from 3 h past sunset until sunrise (average lifetime of 1.6 h) is $\gamma(N_2O_5) = 0.023$. Conversely, case 2 (blue line) shows the predicted lifetime if all reactivity were attributable to NO_3, i.e., for $\gamma(N_2O_5) = 0$. In this case $k(NO_3)$ is 1.4×10^{-3} s^{-1} or a lifetime of approximately 12 min. The large peak in $\tau(N_2O_5)_{calc}$ just before sunset for this case is due to the peak in NO_x at that time (see Figure 4), which leads to a maximum in $K_{eq}[NO_2]$ and in $\tau(N_2O_5)_{calc}$ for $\gamma(N_2O_5) = 0$ using equation (10) (i.e., $\tau(N_2O_5)_{calc}$ proportional to NO_2). Case 3 (red line) shows $\tau(N_2O_5)_{calc}$ for the parameters derived from the average of the nightly fits to the steady state lifetime dependences, $\gamma(N_2O_5) = 0.014$ and $k(NO_3) = 5.6 \times 10^{-4}$. This case is intermediate between the extremes and fits the nighttime average $\tau(N_2O_5)$ equally well. Average $\tau(N_2O_5)$ between 4:00 and 6:30 A.M. is somewhat greater. An uptake coefficient $\gamma(N_2O_5) = 0.005$ approximately fits the data during this time period using $k(NO_3) = 5.6 \times 10^{-4}$ s^{-1}.

Figure 11b shows the average magnitude of loss via NO_3 (blue) and N_2O_5 (red), i.e., the two terms on the right-hand side of equation (10), using the average uptake coefficients and NO_3 loss rate coefficient. The

Table 1. N_2O_5 Uptake Coefficients and NO_3 Loss Rate Coefficients From a Nightly Steady State Analysis

Date	$\gamma(N_2O_5)$	$k(NO_3)$ (10^{-4} s^{-1})
16–17 November	0.022	5.6
17–18 November	0.014	5.8
18–19 November	0.0075	4.6
19–20 November	0.015	8.1
20–21 November	0.011	5.4
21–22 November	0.029	4.3
30 November 30 to 1 December	0.0075	4.9
1–2 December	0.021	1.7
2–3 December	0.010	11
3–4 December	0.004	4.1

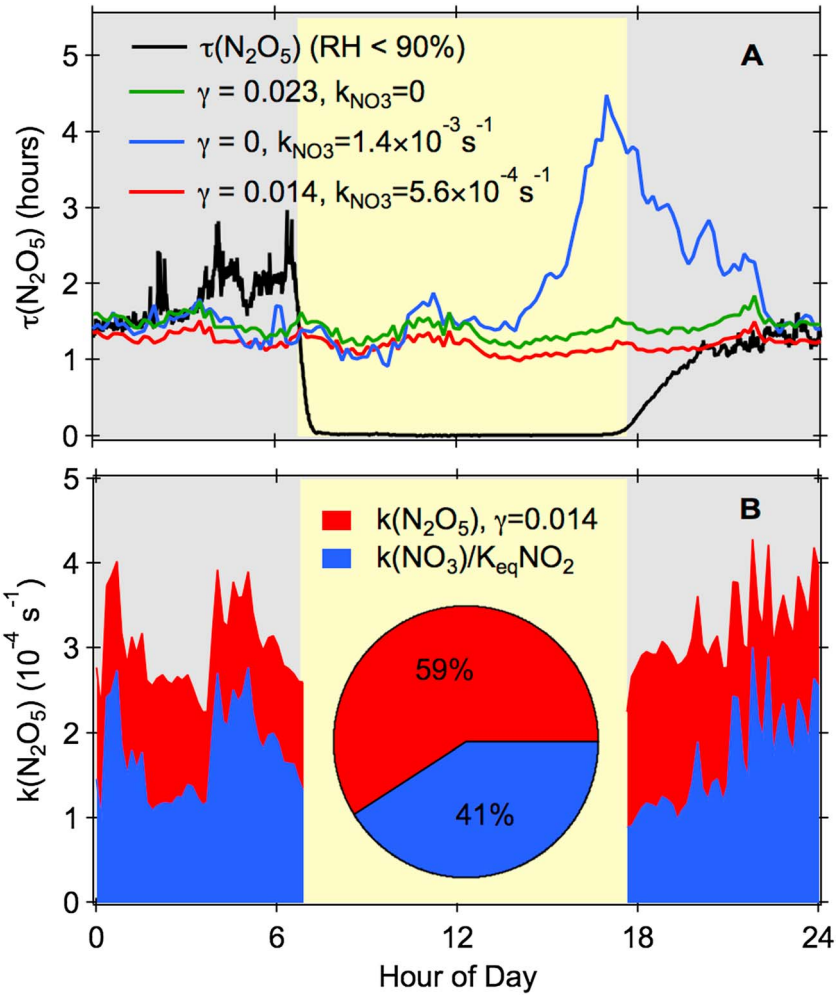

Figure 11. (a) Diel average N_2O_5 lifetime for RH < 90% (black). Also shown are calculated N_2O_5 lifetimes that best match the average for the case of sinks of N_2O_5 only (green), sinks of NO_3 only (blue), and the average of the nightly determinations of $\gamma(N_2O_5)$ and $k(NO_3)$ (red). The legend gives corresponding uptake coefficients and $k(NO_3)$. Calculated values show both daytime and nighttime data, although photochemical reactions of NO_3 dominate the daytime sinks. (b) Average nighttime loss rate coefficients for NO_3 and N_2O_5 using the average nightly $\gamma(N_2O_5)$ and $k(NO_3)$. The $k(NO_3)$ is divided by $K_{eq}[NO_2]$ for direct comparison to $k(N_2O_5)$ (see text). Pie chart in the center shows relative contribution of N_2O_5 and NO_3 sinks.

pie chart in the center of the figure gives the relative contribution of each. They are nearly equal, although N_2O_5 loss accounts for slightly more than half of the total.

4.2. NO_3 Reactivity From Daytime Canister Samples

The first-order loss rate coefficient for NO_3 determined from the nighttime N_2O_5 lifetime analysis can be compared with that determined from measurements of reactive VOCs at the Tai Mo Shan observatory during daytime. The VOC canister measurements were not automated, and nighttime site access restrictions prevented their collection during darkness. A total of 38 canister samples were collected from 27 November to 13 December. Figure 12 shows the average NO_3 first-order loss rate coefficients, $k(NO_3)$, sorted by anthropogenic and biogenic hydrocarbons. The $k(NO_3)$ were calculated from the sum of the products of the bimolecular rate coefficients for reactions of VOCs with NO_3 and the VOC concentrations.

$$k(NO_3) = \sum_i k(NO_3 + VOC_i)[VOC_i] + K_{eq}[NO_2]k(N_2O_5) \quad (11)$$

The second term on the right-hand side of equation (11) is the NO_3 first-order loss rate coefficient through uptake of N_2O_5 [*Brown et al.*, 2003a], shown as the black bar at the bottom of Figure 12 for reference.

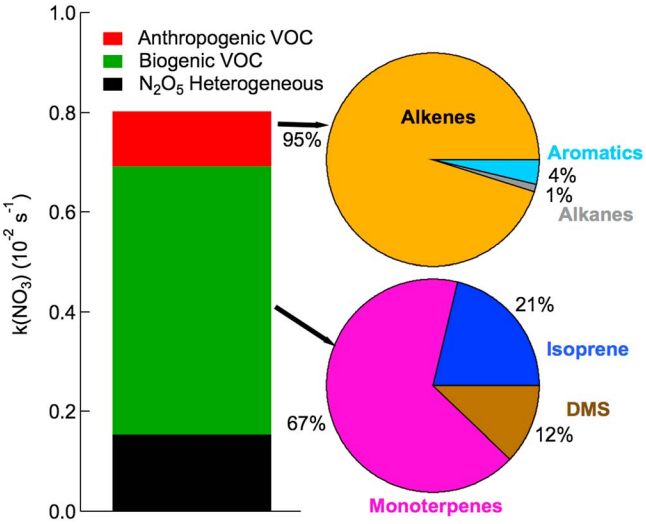

Figure 12. NO_3 reactivity measured from canister samples acquired during daytime. (left) Bar graph shows the average NO_3 summed first-order loss rate coefficient with biogenic and anthropogenic VOCs together with its loss through N_2O_5 uptake using an uptake coefficient of $\gamma(N_2O_5) = 0.014$. (right) Pie charts show the contributions of different categories of VOC to the anthropogenic (top) and biogenic (bottom) components. The $k(NO_3)$ from daytime canister samples is approximately 10 times larger than that inferred from nighttime N_2O_5 lifetimes.

Average daytime $k(NO_3)$ from VOC measurements (excluding loss through N_2O_5) was $6.5 \pm 6.8 \times 10^{-3}$ s^{-1}, equivalent to an NO_3 lifetime of approximately 2.5 min and more than 10 times the average $k(NO_3)$ derived from the nighttime steady state analysis. The much faster NO_3 loss rate is consistent with a substantially less aged air mass that was more influenced by surface level emissions sampled at the mountaintop site during the daytime mixed boundary layer than during the nighttime residual layer. The pie charts on the right-hand side of Figure 12 show the VOC categories that made up the reactivity. Anthropogenic NO_3-VOC reactivity was $1.1 \pm 1.9 \times 10^{-3}$ s^{-1}, twice the total nighttime NO_3 reactivity, and was dominated by anthropogenic alkenes, such as propene and butenes. Aromatics and alkanes made a minor contribution (5%) total. This distribution of NO_3 reactivity with anthropogenic VOCs is similar to that from urban areas in the U.S. [*Brown et al.*, 2011]. Monoterpenes were the dominant component of NO_3-biogenic VOC reactivity, with α- and β-pinene being the only two reported compounds.

Daytime VOC measurements clearly did not reflect the NO_3 reactivity that occurred during the majority of the night but may be indicative of the chemistry occurring during the early hours of the evening during the approximately 3 h time period required for the approach to steady state described above.

5. Daytime N_2O_5

Although NO_3 and N_2O_5 normally occur in large concentrations only at night in the lower troposphere, they are present at small but nonzero levels during daytime. Several studies have reported measurements of daytime NO_3 or N_2O_5 from ground sites [*Geyer et al.*, 2003], ships [*Osthoff et al.*, 2006], and aircraft [*Brown et al.*, 2005] in the U.S., as well as from a lower altitude site in Hong Kong [*Wang et al.*, 2014]. During the 2013 Tai Mo Shan study, the largest NO_x and least aged urban emissions occurred during late afternoon (Figure 4) and early evening, such that the largest $P(NO_3)$ and potentially most active NO_3 and N_2O_5 chemistry occurred during this time of day. Figure 13 shows the diel average N_2O_5 plotted on a logarithmic scale to illustrate the small but nonzero daytime mixing ratio, which varied between 1 and 2 pptv between 9:00 and 14:00. From 14:00 to 19:00, N_2O_5 mixing ratios rose continuously to an average maximum of ~350 pptv near 19:00, with an average sunset mixing ratio of ~60 pptv. Also shown in Figure 13 is the calculated daytime N_2O_5 predicted from a steady state between production through reactions (1) and (2) and loss through NO_3 photolysis and reaction with NO (reactions (12) and (13) below).

$$NO_3 + h\nu \rightarrow \text{products}(NO_2 + O \text{ or } NO + O_2) \quad (12)$$

$$NO_3 + NO \rightarrow 2NO_2 \quad (13)$$

The rate coefficient for reaction (13) is rapid ($k = 2.6 \times 10^{-11}$ cm^3 $molecule^{-1}$ s^{-1} at 298 K [*Sander et al.*, 2011]), such that reaction (13) is more rapid than NO_3 photolysis in determining daytime levels of NO_3 and N_2O_5 for NO above approximately 0.3 ppbv. If other loss processes for NO_3 and N_2O_5 are small compared to reactions (12) and (13), equation (14) gives the predicted daytime steady state in N_2O_5 [*Brown et al.*, 2005].

$$N_2O_5(\text{Day}) = K_{eq}[NO_2]\frac{P(NO_3)}{j(NO_3) + k_{13}[NO]} \quad (14)$$

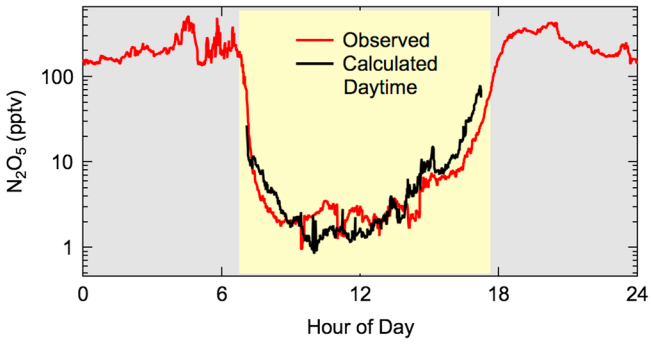

Figure 13. Diel average N_2O_5 on a logarithmic scale (red) together with a calculation of daytime (solar elevation angle > 5°) average N_2O_5 according to equation (14).

Here $j(NO_3)$ is the first-order photolysis rate coefficient for reaction (12), for which there were no direct measurements. Photolysis rate coefficients for NO_2 were measured, and $j(NO_3)$ was calculated based on its correlation with $j(NO_2)$ from aircraft data during the TexAQS 2006 campaign [*Parrish et al.*, 2008]. The estimated error in deriving $j(NO_3)$ from this correlation is ±30%. The black line in Figure 13 shows the average calculated daytime N_2O_5 (arbitrarily defined here as solar elevation angle > 5° to avoid periods near dawn and dusk) for comparison to observation. The calculation has the same pattern as the observations and is of the same magnitude (1–2 pptv) through the morning and early afternoon hours. During the late day rise in N_2O_5, the calculation overpredicts the observation, possibly indicating that sinks other than reactions (12) and (13) are important during late afternoon, when NO_3 production rates are largest.

Figure 14 shows the same comparison for two individual days, 27 November and 30 November, to illustrate the influence of daytime N_2O_5 heterogeneous uptake. Both days had large afternoon $P(NO_3)$. On 30 November there was sustained $P(NO_3)$ of 2–3 ppbv h^{-1}, while 27 November had $P(NO_3)$ of 1–2 ppbv h^{-1} with a sharp maximum above 3.5 ppbv h^{-1}. On 30 November, the observed and calculated late afternoon N_2O_5 values agree well, with the observations on average 80% of the calculation (i.e., observations 20% lower than the calculation) between 14:00 and sunset. On 27 November, by contrast, observations are much smaller, adding up to only 5% of the calculation during the same period of the day, suggesting that 95% of the NO_3 and N_2O_5 sinks were other than reactions (12) and (13). Relative humidity was saturated at 100% on 27 November, indicating that the site was impacted by fog at that time. Uptake of N_2O_5 to fog droplets is thus a likely candidate for the discrepancy [*Lelieveld and Crutzen*, 1990]. If the dominant (95%) loss process for N_2O_5 during this late afternoon event were

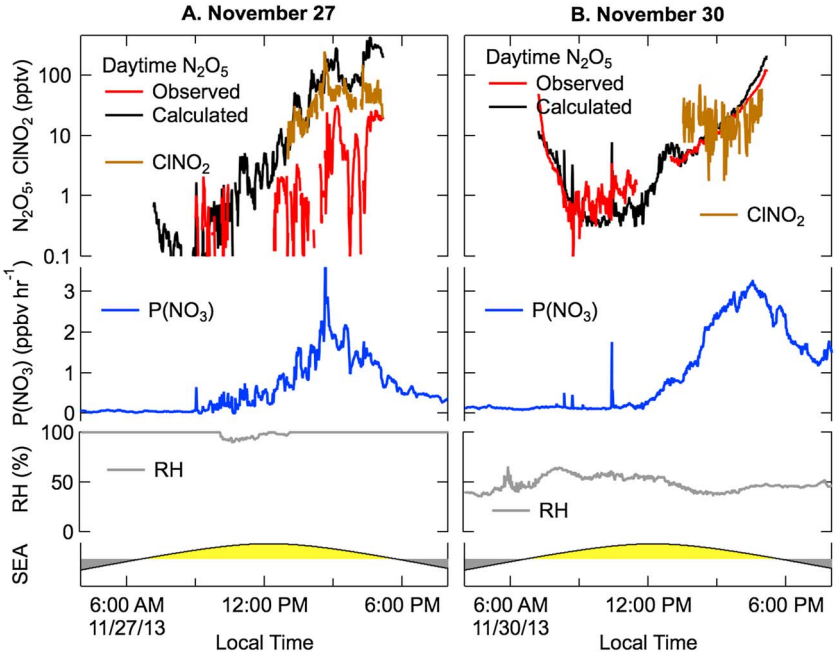

Figure 14. Observed and calculated daytime N_2O_5 and observed $ClNO_2$ (for the time period when these data were available), nitrate radical production rate, and relative humidity for (a) 27 November and (b) 30 November. Bottom plots show solar elevation angle (SEA) for reference of day and night.

through heterogeneous uptake, the resulting conversion of NO_x to soluble nitrate and/or $ClNO_2$ would proceed at twice the nitrate radical production rate, or 2.7 ppbv h^{-1}. For reference, reaction of OH with NO_2 at the observed concentration would proceed at approximately 1 ppbv h^{-1}, assuming a late afternoon OH concentration of 2×10^6 cm^{-3}. Thus, daytime production of soluble nitrate via N_2O_5 can be substantially faster than photochemical conversion through $OH + NO_2$ in the polluted clouds that impact this mountaintop observatory.

Figure 14 also shows the $ClNO_2$ product from N_2O_5 uptake during daylight hours for both days. On the high RH/fog day, $ClNO_2$ follows calculated N_2O_5 production and significantly exceeds N_2O_5 itself. The apparent agreement between $ClNO_2$ and calculated N_2O_5 is fortuitous, however, since there is no daytime steady state in $ClNO_2$ that is analogous to N_2O_5. Rather, $ClNO_2$ more nearly represents its integrated production. At an average afternoon mixing ratio of 50 pptv, $ClNO_2$ is likely much smaller than soluble nitrate, which would be produced rapidly at the rate given above. The observation of a small $ClNO_2$ mixing ratio under conditions of rapid nitrate production via N_2O_5 is consistent with a small $ClNO_2$ yield in fog droplets that consist mainly of water [*Bertram and Thornton*, 2009; *Roberts et al*., 2009]. On the low-RH day, $ClNO_2$ is present at a mixing ratio approximately equal to or smaller than that of N_2O_5, likely as the result of much less rapid N_2O_5 heterogeneous uptake but potentially larger $ClNO_2$ yield. Daytime heterogeneous chemistry of N_2O_5 may therefore be a small source of photolabile chlorine under both dry and wet conditions, although it would provide a large source of soluble nitrate in wet but not dry conditions. The companion paper presents a much more extensive analysis of the nighttime characteristics of $ClNO_2$ and its influence on next-day photochemistry [*Wang et al*., 2016].

6. Conclusions

We report the first observations of the nighttime nitrogen oxides, NO_3 and N_2O_5, from a site in the residual layer in China. Observations took place at Tai Mo Shan, a mountaintop observatory in Hong Kong and within the Pearl River Delta region. Although the site was high enough (957 m) to periodically sample from above the daytime mixed boundary layer, it was always influenced by at least moderate NO_x pollution. Maximum nightly mixing ratios of N_2O_5 were generally in the range of 0.5–4 ppbv on nights without significant influence of fog but were observed at 7.8 ppbv (1 min average) and 11.8 ppbv (1 s average) during one large event. The event exhibited large variability observable in measurements with 1 s time resolution and possibly driven by sampling from a poorly mixed air pollution plume advecting over the mountaintop site. Although intense urban pollution events were infrequent at Tai Mo Shan due to the prevailing easterly air flow at this site, the large nighttime plume intercepts were likely indicative of the typical characteristics of nighttime urban outflow from the megacities of the Pearl River Delta.

Analysis of the NO_x and aerosol dependence of the N_2O_5 steady state lifetime yielded an average uptake coefficient to aerosol of $\gamma(N_2O_5) = 0.014 \pm 0.007$, although the uncertainty does not likely represent the full range of potential variability in this uptake coefficient. This number is likely an upper limit due to potential artifacts in the determination method. Nighttime average NO_3 loss rate coefficients were determined to be slow, equivalent to an NO_3 lifetime longer than 30 min in aged air sampled at the mountaintop site. Even with the slower loss rate coefficient for NO_3, sinks of NO_3 and N_2O_5 each contributed approximately equally to the total loss rate of the pair of compounds. Analysis of NO_3 reactivity (approximately 2.5 min average lifetime) in canister samples collected during daytime showed a much larger loss rate for NO_3 to VOCs present in less aged air measured during daylight hours, indicating considerable potential for NO_3 oxidation chemistry within plumes closer to large emission sources at night. Finally, observations of small daytime N_2O_5 mixing ratios were consistent with its predicted photochemical steady state in an average sense. Observations during daytime polluted fog suggested a large discrepancy between observed and calculated N_2O_5 and an important role for heterogeneous uptake of N_2O_5 in cloud as a source of soluble nitrate during daytime.

Acknowledgments

S.S.B., W.P.D., and D.D.P. acknowledge support from the NOAA Atmospheric Chemistry, Climate and Carbon Cycle (AC4) program for this work. The Hong Kong team acknowledges support from the Hong Kong Research Grants Council (PolyU 153026/14P), the Hong Kong Environmental Protection Department, and the Hong Kong Polytechnic University. The authors would like to thank Xu Zheng and Wang Xinfeng for their support in setting up the site and to Peter K.K. Louie' and Connie W.Y. Luk for their help with access to the TMS site and for providing some TMS local wind data. Data are available upon request (steven.s.brown@noaa.gov, tao.wang@polyu.edu.hk).

References

Atkinson, R., A. M. Winer, and J. N. Pitts Jr. (1986), Estimation of night-time N_2O_5 concentrations from ambient NO_2 and NO_3 radical concentrations and the role of N_2O_5 in night-time chemistry, *Atmos. Environ. 20*(2), 331–339.

Benton, A. K., J. M. Langridge, S. M. Ball, W. J. Bloss, M. Dall'Osto, E. Nemitz, R. M. Harrison, and R. L. Jones (2010), Night-time chemistry above London: Measurements of NO_3 and N_2O_5 from the BT Tower, *Atmos. Chem. Phys. 10*(20), 9781–9795, doi:10.5194/acp-10-9781-2010.

Bertram, T. H., and J. A. Thornton (2009), Toward a general parameterization of N_2O_5 reactivity on aqueous particles: The competing effects of particle liquid water, nitrate and chloride, *Atmos. Chem. Phys. 9*, 8351–8363.

Brown, S. S., and J. Stutz (2012), Nighttime radical observations and chemistry, *Chem. Soc. Rev. 41*, 6405–6447, doi:10.1039/c2cs35181a.

Brown, S. S., H. Stark, and A. R. Ravishankara (2003a), Applicability of the steady-state approximation to the interpretation of atmospheric observations of NO_3 and N_2O_5, *J. Geophys. Res.*, *108*(D17), 4539, doi:10.1029/2003JD003407.

Brown, S. S., H. Stark, T. B. Ryerson, E. J. Williams, D. K. J. Nicks, M. Trainer, F. C. Fehsenfeld, and A. R. Ravishankara (2003b), Nitrogen oxides in the nocturnal boundary layer: Simultaneous, in-situ detection of NO_3, N_2O_5, NO, NO_2 and O_3, *J. Geophys. Res.*, *108*(D9), 4299, doi:10.1029/2002JD002917.

Brown, S. S., et al. (2004), Nighttime removal of NO_x in the summer marine boundary layer, *Geophys. Res. Lett.*, *31*, L07108, doi:10.1029/2004GL019412.

Brown, S. S., et al. (2005), Aircraft observations of daytime NO_3 and N_2O_5 and their implications for tropospheric chemistry, *J. Photochem. Photobiol. A*, *176*(1–3), 270–278.

Brown, S. S., et al. (2006a), Nocturnal odd-oxygen budget and its implications for ozone loss in the lower troposphere, *Geophys. Res. Lett.*, *33*, L08801, doi:10.1029/2006GL025900.

Brown, S. S., et al. (2006b), Variability in nocturnal nitrogen oxide processing and its role in regional air quality, *Science*, *311*, 67–70.

Brown, S. S., et al. (2007), Vertical profiles in NO_3 and N_2O_5 measured from an aircraft: Results from the NOAA P-3 and surface platforms during NEAQS 2004, *J. Geophys. Res.*, *112*, D22304, doi:10.1029/2007JD008883.

Brown, S. S., et al. (2009), Reactive uptake coefficients for N_2O_5 determined from aircraft measurements during TexAQS 2006: Comparison to current model parameterizations, *J. Geophys. Res.*, *114*, D00F10, doi:10.1029/2008JD011679.

Brown, S. S., et al. (2011), Budgets for nocturnal VOC oxidation by nitrate radicals aloft during the 2006 Texas Air Quality Study, *J. Geophys. Res.*, *116*, D24305, doi:10.1029/2011JD016544.

Cooper, O. R., R.-S. Gao, D. Tarasick, T. Leblanc, and C. Sweeney (2012), Long-term ozone trends at rural ozone monitoring sites across the United States, 1990–2010, *J. Geophys. Res.*, *117*, D22307, doi:10.1029/2012JD018261.

Crowley, J. N., G. Schuster, N. Pouvesle, U. Parchatka, H. Fischer, B. Bonn, H. Bingemer, and J. Lelieveld (2010), Nocturnal nitrogen oxides at a rural mountain-site in south-western Germany, *Atmos. Chem. Phys. 10*(6), 2795–2812.

Day, D. A., M. B. Dillon, P. J. Wooldridge, J. A. Thornton, R. S. Rosen, E. C. Wood, and R. C. Cohen (2003), On alkyl nitrates, O_3, and the "missing NO_y", *J. Geophys. Res.*, *108*(D16), 4501, doi:10.1029/2003JD003685.

Draxler, R. R., and G. D. Rolph (2003), HYSPLIT (HYbrid Single-Particle Lagrangian Integrated Tracker) Model access via NOAA ARL Ready Website [Available at http://www.arl.noaa.gov/ready/hysplit4.html, NOAA Air Resources Laboratory, Silver Spring, MD].

Fuchs, H., W. P. Dubé, S. J. Ciciora, and S. S. Brown (2008), Determination of inlet transmission and conversion efficiencies for in situ measurements of the nocturnal nitrogen oxides, NO_3, N_2O_5 and NO_2, via pulsed cavity ring-down spectroscopy, *Anal. Chem. 80*(15), 6010–6017, doi:10.1021/ac8007253.

Geyer, A., et al. (2003), Direct observations of daytime NO_3: Implications for urban boundary layer chemistry, *J. Geophys. Res.*, *108*(D12), 4368, doi:10.1029/2002JD002967.

Guo, S., et al. (2014), Elucidating severe urban haze formation in China, *Proc. Natl. Acad. Sci. U. S. A. 111*(49), 17,373–17,378.

Hilboll, A., A. Richter, and J. P. Burrows (2013), Long-term changes of tropospheric NO_2 over megacities derived from multiple satellite instruments, *Atmos. Chem. Phys. 13*(8), 4145–4169, doi:10.5194/acp-13-4145-2013.

Huang, R.-J., et al. (2014), High secondary aerosol contribution to particulate pollution during haze events in China, *Nature*, advance online publication, doi:10.1038/nature13774.

Kennedy, O. J., et al. (2011), An aircraft based three channel broadband cavity enhanced absorption spectrometer for simultaneous measurements of NO_3, N_2O_5 and NO_2, *Atmos. Meas. Tech. 4*, 1759–1776, doi:10.5194/amtd-4-3499-2011.

Lelieveld, J., and P. J. Crutzen (1990), Influences of cloud photochemical processes on tropospheric ozone, *Nature*, *343*, 227–233.

Osthoff, H. D., et al. (2006), Observations of daytime N_2O_5 in the marine boundary layer during New England Air Quality Study—Intercontinental Transport and Chemical Transformation 2004, *J. Geophys. Res.*, *111*, D23S14, doi:10.1029/2006JD007593.

Osthoff, H. D., M. J. Pilling, A. R. Ravishankara, and S. S. Brown (2007), Temperature dependence of the NO_3 absorption cross section above 298 K and determination of the equilibrium constant for $NO_3 + NO_2 <--> N_2O_5$ at atmospherically relevant conditions, *Phys. Chem. Chem. Phys. 9*, 5785–5793, doi:10.1039/b709193a.

Parrish, D. D., et al. (2008), Overview of the Second Texas Air Quality Study (TexAQS II) and the Gulf of Mexico Atmospheric Composition and Climate Study (GoMACCS), *J. Geophys. Res.*, *114*, D00F13, doi:10.1029/2009JD011842.

Pathak, R. K., W. S. Wu, and T. Wang (2009), Summertime $PM_{2.5}$ ionic species in four major cities of China: Nitrate formation in an ammonia-deficient atmosphere, *Atmos. Chem. Phys. 9*, 1711–1722.

Pathak, R. K., T. Wang, and W. S. Wu (2011), Nighttime enhancement of $PM_{2.5}$ nitrate in ammonia-poor atmospheric conditions in Beijing and Shanghai: Plausible contributions of heterogeneous hydrolysis of N_2O_5 and HNO_3 partitioning, *Atmos. Environ. 45*(5), 1183–1191.

Platt, U., G. LeBras, G. Poulet, J. P. Burrows, and G. Moortgat (1990), Peroxy radicals from night-time reactions of NO_3 with organic compounds, *Nature*, *348*, 147–149.

Platt, U. F., A. M. Winer, H. W. Bierman, R. Atkinson, and J. N. Pitts Jr. (1984), Measurement of nitrate radical concentrations in continental air, *Environ. Sci. Technol. 18*, 365–369.

Pye, H. O. T., A. W. H. Chan, M. P. Barkley, and J. H. Seinfeld (2010), Global modeling of organic aerosol: The importance of reactive nitrogen (NO_x and NO_3), *Atmos. Chem. Phys. 10*(22), 11,261–11,276, doi:10.5194/acp-10-11261-2010.

Roberts, J. M., H. D. Osthoff, S. S. Brown, and A. R. Ravishankara (2009), Laboratory studies of products of N_2O_5 uptake on Cl^- containing substrates, *Geophys. Res. Lett.*, *36*, L20808, doi:10.1029/2009GL040448.

Russell, A. R., L. C. Valin, and R. C. Cohen (2012), Trends in OMI NO_2 observations over the United States: Effects of emission control technology and the economic recession, *Atmos. Chem. Phys. 12*(24), 12,197–12,209, doi:10.5194/acp-12-12197-2012.

Sander, S. P., et al. (2011), *Chemical Kinetics and Photochemical Data for Use in Atmospheric Studies*, JPL Publication 10–6, Pasadena, Calif.

Simon, H., A. Reff, B. Wells, J. Xing, and N. Frank (2014), Ozone trends across the United States over a period of decreasing NO_x and VOC emissions, *Environ. Sci. Technol. 49*(1), 186–195, doi:10.1021/es504514z.

Stull, R. B. (1988), *An Introduction to Boundary Layer Meteorology*, Kluwer Academic, Dordrecht, Netherlands.

Stutz, J., B. Alicke, R. Ackermann, A. Geyer, A. B. White, and E. Williams (2004), Vertical profiles of NO_3, N_2O_5, O_3, and NO_x in the nocturnal boundary layer: 1. Observations during the Texas Air Quality Study 2000, *J. Geophys. Res.*, *109*, D12306, doi:10.1029/2003JD004209.

Tang, G., X. Li, Y. Wang, J. Xin, and X. Ren (2009), Surface ozone trend details and interpretations in Beijing, 2001–2006, *Atmos. Chem. Phys. 9*(22), 8813–8823.

Thornton, J. A., et al. (2010), A large atomic chlorine source inferred from mid-continental reactive nitrogen chemistry, *Nature*, *464*, 271–274.

Wagner, N. L., W. P. Dubé, R. A. Washenfelder, C. J. Young, I. B. Pollack, T. B. Ryerson, and S. S. Brown (2011), Diode laser-based cavity ring-down instrument for NO_3, N_2O_5, NO, NO_2 and O_3 from aircraft, *Atmos. Meas. Tech. 4*, 1227–1240.

Wagner, N. L., et al. (2013), N_2O_5 uptake coefficients and nocturnal NO_2 removal rates determined from ambient wintertime measurements, *J. Geophys. Res. Atmos. 118*, 9331–9350, doi:10.1002/jgrd.50653.

Wang, S., C. Shi, B. Zhou, H. Zhao, Z. Wang, S. Yang, and L. Chen (2013), Observation of NO_3 radicals over Shanghai, China, *Atmos. Environ. 70*, 401–409, doi:10.1016/j.atmosenv.2013.01.022.

Wang, T., A. Ding, J. Gao, and W. S. Wu (2006), Strong ozone production in urban plumes from Beijing, China, *Geophys. Res. Lett.*, *33*, L21806, doi:10.1029/22006GL027689.

Wang, T., X. L. Wei, A. J. Ding, C. N. Poon, K. S. Lam, Y. S. Li, L. Y. Chan, and M. Anson (2009), Increasing surface ozone concentrations in the background atmosphere of Southern China, 1994–2007, *Atmos. Chem. Phys. 9*(16), 6217–6227.

Wang, T., et al. (2016), Observations of nitryl chloride and modeling its source and effect on ozone in the planetary boundary layer of southern China, *J. Geophys. Res. Atmos.*, *121*, doi:10.1002/2015JD024556.

Wang, X., T. Wang, C. Yan, Y. J. Tham, L. Xue, Z. Xu, and Q. Zha (2014), Large daytime signals of N_2O_5 and NO3 inferred at 62 amu in a TD-CIMS: Chemical interference or a real atmospheric phenomenon? *Atmos. Meas. Tech. 7*(1), 1–12, doi:10.5194/amt-7-1-2014.

Winer, A. M., R. Atkinson, and J. N. J. Pitts (1984), Gaseous nitrate radical: Possible nighttime atmospheric sink for biogenic organic compounds, *Science*, *224*, 156–158.

Xue, J., Z. Yuan, A. K. H. Lau, and J. Z. Yu (2014), Insights into factors affecting nitrate in $PM_{2.5}$ in a polluted high NO_x environment through hourly observations and size distribution measurements, *J. Geophys. Res. Atmos. 119*, 4888–4902, doi:10.1002/2013JD021108.

Yang, D., C. Li, A. K. H. Lau, and Y. Li (2013), Long-term measurement of daytime atmospheric mixing layer height over Hong Kong, *J. Geophys. Res. Atmos. 118*, 2422–2433, doi:10.1002/jgrd.50251.

Zheng, B., Q. Zhang, Y. Zhang, K. B. He, K. Wang, G. J. Zheng, F. K. Duan, Y. L. Ma, and T. Kimoto (2015), Heterogeneous chemistry: a mechanism missing in current models to explain secondary inorganic aerosol formation during the January 2013 haze episode in North China, *Atmos. Chem. Phys. 15*(4), 2031–2049, doi:10.5194/acp-15-2031-2015.